An Ultra-Low-Power Biomedical Chip for Injectable Pressure Monitor

Inhee Lee[1], Wanyeong Jung[1], Hyunsoo Ha[2], Seokhyeon Jeong[1], Yejoong Kim[1], Gyouho Kim[1], Zhiyoong Foo[1], Jae-Yoon Sim[2], Dennis Sylvester[1], and David Blaauw[1]
[1]University of Michigan, Ann Arbor, USA
[2]Pohang University of Science and Technology, Pohang, Korea

***Abstract*—Implantable pressure monitors enable diagnosis and track patient health or disease progression in different organs such as the brain, eye, heart, and bladder. Miniaturization of the implantable sensors helps reduce patient pain and recovery time, decrease foreign body rejection, and allow the device to be placed in limited spaces. This paper explores a miniaturized pressure monitor which can even be injected through a syringe. Required specifications are investigated to develop the small pressure monitor. Also, low-power circuit techniques to meet extremely small power budget are discussed for a capacitive-to-digital converter, an energy harvester, and digital circuits.**

I. Introduction

Pressure is an important indicator of patient health or disease progression since it is highly regulated in various organs of the body such as the brain, eye, heart, and bladder [1]. The absolute pressure value and its variation provides information to diagnose the progress of medical intervention. For example, intraocular pressure (IOP) is a primary contributing factor for glaucoma. It normally ranges between 10 to 21 mmHg. Only currently available therapeutic modality for glaucoma is adjusting the value by medications or surgery to the normal range [2].

Typically, the pressure is measured in the clinic as a single data point. Thus, important peak or trough values, or changes in the profile, can be missed. Also, the measurement results can be perturbed when a patient visits the clinic due to stress [1]. To solve these issues, the possibilities of an implantable pressure sensor have been explored. An implantable pressure sensor enables pressure to be monitored in a patient's normal life style over the lifetime of the implanted sensor in the patient.

The implantable device becomes more effective with smaller form factors. Compared to a larger sensor, a smaller sensor could be implanted by a less invasive surgery, while allowing devices to be placed in new locations with limited space and enabling new treatment procedures for diseases like glaucoma [3]. A smaller device also reduces foreign body rejection and becomes more biocompatible.

Implantable passive LC resonant circuits have shown small form factor ($2\times3.4\times15mm^3$ [4] and $4\times1mm^2$ [5]), but they can only monitor and record the pressure with external RF transceivers. Recently developed active implantable pressure sensors offer continuous functionality even when the external device is not available [6]-[7]. But the available average power budget of such devices is extremely limited due to the small sensor form factor that reduces the maximum energy stored in a capacitor or a battery. In this paper, we explore ultra-low-power circuit design techniques to enable miniaturization of such implantable pressure sensor systems for syringe-injected therapeutic systems.

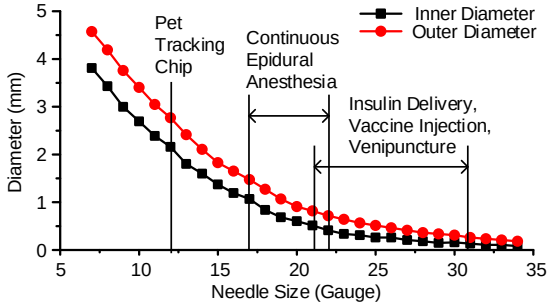

Fig. 1. Inner and outer diameters over needle gauge.

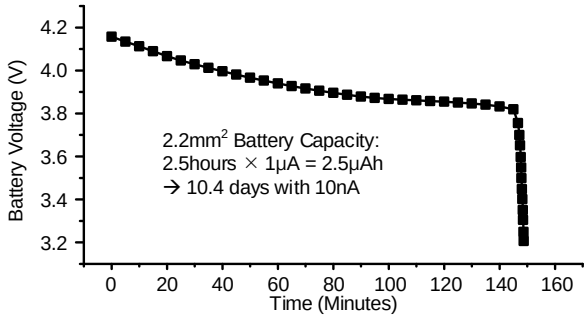

Fig. 2. Measured battery discharge curve with 1μA.

II. Requirements of Injectable Pressure Monitor

Fig. 1 shows inner and outer dimensions of different syringes. mm-scale in diameter is acceptable, but a smaller needle size is desirable considering patient's pain and recovery time [8]. To be injected through a syringe, the battery size is limited to ~1mm, considering an additional size increment due to biocompatible packaging.

Fig. 2 shows a measured thin-lithium battery ($1.0\times2.2mm^2$) with 1μA discharging current. The 2.5μAh battery capacity offers the 10.4-day lifetime with extremely small current consumption of 10nA (e.g. typically ~μA). An energy harvester helps increase the lifetime and eventually enables energy autonomous operation. However, the area constraint on the energy source size limits its performance. For example, $0.84mm^2$ photovoltaic cells offers only 7nW with indoor light condition (260lux) [9]. Thus, ultra-low-power circuits and an energy-efficient energy harvester even at low energy condition are necessary to develop the injectable pressure monitor.

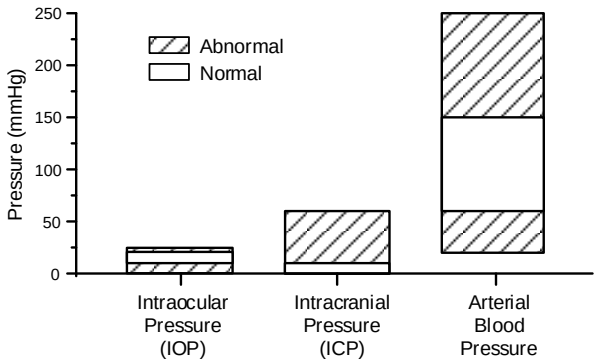

Fig. 3. Required pressure range for different applications.

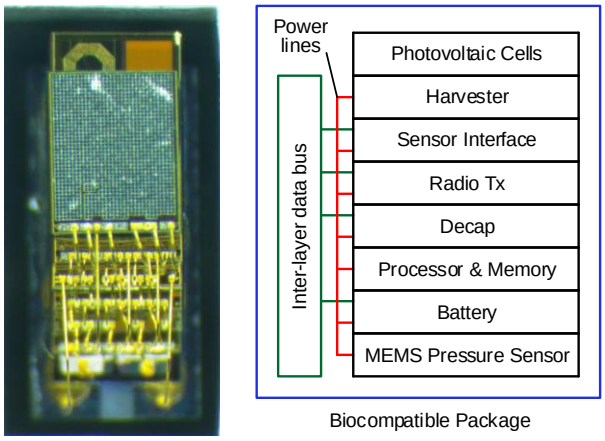

(a) (b)

Fig. 4. Proposed injectable pressure sensor (a) Photograph (b) Sensor block diagram.

Despite the limited power budget, the sensors must be able to measure target pressures with required range and precision. Fig. 3 shows required pressure range for different implantable applications [1], [2]. 1mmHg or 5%−10% of the clinically normal range is commonly accepted for sensor precision [1].

III. Proposed Injectable Pressure Monitor

To satisfy these requirements, we have developed an ultra-low-power injectable pressure sensor as shown in Fig. 4 (a). Its size is $1.6\times2.0\times3.2\text{mm}^3$ including a package, which is $4.6\times$ less than the volume of an injectable RFID chip for pet identification (47.0mm^3, DATAMARS). For optimizing circuit performance, dies from different technologies are stacked and wire-bonded together [7]. The stacked multi-layer structure allows more silicon area per unit volume and enables the system to address different applications by swapping layers in and out for flexibility in system configuration.

In this system, the Murata capacitive pressure sensor converts pressure to capacitance, and the 160nW 64fJ/conversion-step capacitive-to-digital converter (CDC) digitizes the capacitance to a digital code. The 3nW self-starting energy harvester charges the Cymbet thin-film lithium battery using CMOS photovoltaic cells. Also, an ARM M0 processor with a 3kB retentive SRAM manage the sensing operation.

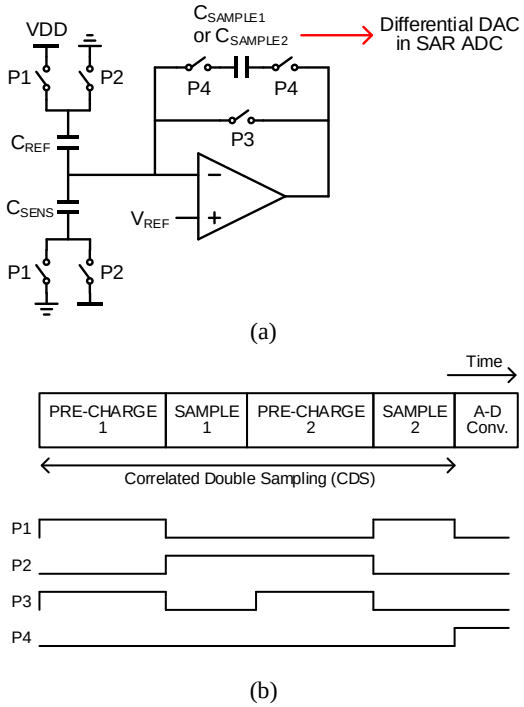

Fig. 5. Readout frontend for CDS in CDC (a) Circuit Diagram (b) CDC operation sequence and signals for switches.

IV. Ultra-Low-Power Circuit Design

In this section, the low-power CDC and energy harvester are discussed, in addition to ultra-low-power digital techniques for enhancing energy efficiency are discussed.

A. *160nW 64fJ/conversion-step CDC*

Typical CDCs are based on a switched-capacitor ΔΣ converter. A switched-capacitor ΔΣ converter achieves high resolution by oversampling, but it results in poor energy efficiency since the oversampling requirement necessitates the modulator filter to operate at a much higher frequency than the CDC conversion speed and the input sampler to charge a large sensor capacitor repeatedly. Thus, this type of converter is not suited to duty-cycled low-power sensors since it requires numerous cycles for the first result. A CDC using successive approximation is proposed for the intermittent operation, but it reduces voltage swing at the input of the comparator by directly connecting the large sensor capacitor to the capacitor DAC and degrades the achievable effective number of bits [10].

This problem is addressed in [11] by using a readout frontend with correlated double sampling (CDS) as shown in Fig. 5 (a). The negative input voltage is forced to reference voltage (V_{REF}) by an amplifier as virtual ground. Charge proportional to '$C_{SENS} - C_{REF}$' is transferred to the sampling capacitor ($C_{SAMPLE1}$ or $C_{SAMPLE2}$) by alternatively connecting the reference capacitor (C_{REF}) and sensor capacitor (C_{SENS}) to supply voltage or ground, as shown in Fig. 5 (b).

The repeated charge transfer operations with the opposite polarity store the output values, including sensor capacitance information as differential format in $C_{SAMPLE1}$ or $C_{SAMPLE2}$. This

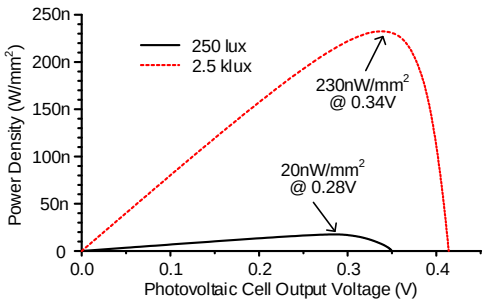

Fig. 6. Measured CMOS photovoltaic cell.

can reduce the effect of low-frequency variation, noise, and offset from the V_{REF} and amplifier. After the CDS process, $C_{SAMPLE1}$ and $C_{SAMPLE2}$ are used as a differential capacitive DAC for the SAR A-to-D conversion. The CDC achieves an effective number of bits of 13.3b with a resolution of 6.0fF. Also, combined with a pressure sensor, it demonstrates a resolution of 0.4mmHg, which satisfies the required precision mentioned above.

The output value of the CDC is relative to C_{REF}. For a given C_{REF}, C_{SENS} from $C_{REF} - C_{SAMPLEX}/4$ to $C_{REF} + C_{SAMPLEX}/4$ is covered. The C_{REF} can be changed with capacitors connected in parallel with switches to cover various capacitive sensors for different applications. 1pF is overlapped between neighboring C_{REF}s to avoid an oscillation problem. With a 3b code, C_{REF} can be changed from 7.5pF to 70.5pF in 9pF steps, which offers input capacitance range of 2.5 ~ 7.53pF for C_{SENS}.

B. 3nW self-starting capacitive energy harvester

Fig. 6 shows measured results with CMOS photovoltaic cells. Due to size constraint of the injectable sensor, energy from a source is also limited. To charge a battery with < 1mm^2 photovoltaic cells in indoor conditions (~200lux), an energy harvester with <10nW is required. Typically, boost DC DC converters are used with high conversion efficiency, but they need large off-chip inductors for low input power levels. Switched-capacitor DC DC converters can be easily integrated with on-chip capacitors. However, their efficient operation have been constrained to µW power conversion due to overhead from clock generation and level-conversion to drive power switches.

The fully integrated energy harvester proposed in [9] removes the overhead and converts 7nW input power from 250mV to 4V in low light condition (260lux) by using 0.84mm^2 CMOS photovoltaic cells. It is enabled by a self-oscillating voltage doubler and a reconfigurable energy harvester architecture.

Fig. 7 (a) shows the proposed voltage doubler with two stacked ring oscillators and flying capacitor (C_{FLY}) connecting their outputs. The stacked inverters in the rings drive the next stage and transfer power from lower ring supply (V_{MED}) to upper ring supply (V_{HIGH}) by charging/discharging C_{FLY}. For the optimum conversion efficiency by balancing switching and conduction losses, a tunable leakage-based delay element and a pass transistor are inserted between stages. The output voltage is set to 58% of the input voltage by controlling V_{CTRL} of the pass transistor and thus the operating frequency of the DC DC converter. For varying input power, the frequency is

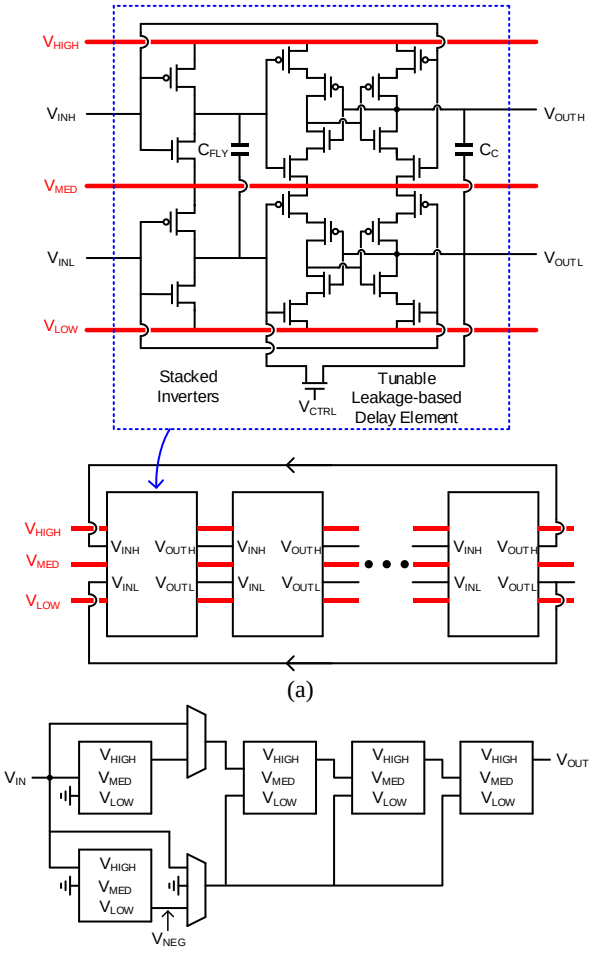

Fig. 7. Low-power energy harvester (a) Self-oscillating voltage doubler (b) Energy harvester architecture.

automatically adjusted with a voltage divider, a comparator, and an internal charge pump to generate V_{CTRL}.

Fig. 7 (b) shows the reconfigurable energy harvester architecture using the five voltage doublers. To increase the available number of voltage conversion ratio, a negative voltage (V_{NEG}) is generated by assigning the energy source output (V_{IN}) and ground to V_{HIGH} and V_{MED}, respectively. Different types of transistors are used for the voltage doublers, considering voltage levels. By setting V_{LOW} of the right three voltage doublers to V_{IN}, ground, or V_{NEG}, the voltage conversion ratio can be changed from 9× to 23×. For cold start operation, the control logic is placed between V_{IN} and V_{NEG}.

C. Energy-efficient Microprocessor and Low-lekage Memory

On-chip data processing with a microprocessor allows the system to extract and compress data for better energy efficiency. It avoids storing and transmitting raw measurement data, of which only a small portion is typically useful.

For the limited energy budget of the injectable sensor, energy consumed in the microprocessor can be saved with lower supply voltage since dynamic switching energy quadratically scales with the supply voltage. Instead, leakage

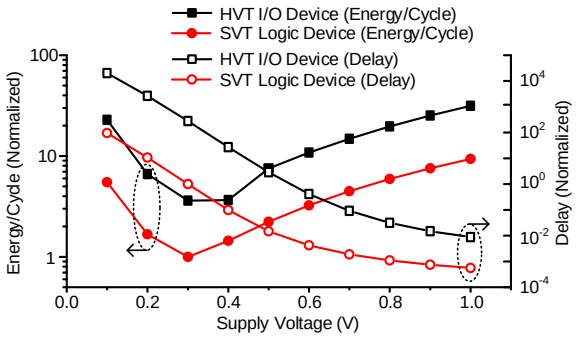

Fig. 8. Simulated energy/cycle and delay over supply voltage.

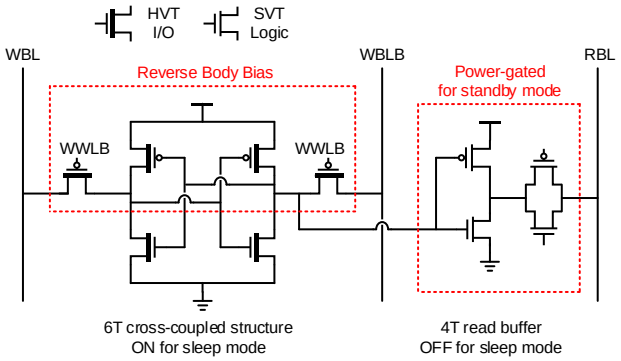

Fig. 9. Circuit diagram for low-leakage 10T SRAM.

energy per cycle increases due to exponentially increased delay below the device threshold voltage (V_{TH}). From the trade-off between dynamic and leakage energy, as shown in Fig. 8, the optimum supply voltage for standard V_{TH} (SVT) logic transistor energy exists near V_{TH} [12]. I/O transistors with ~0.7V V_{TH} have relatively low energy-efficient supply voltage due to smaller leakage.

However, in low supply voltage, a reduced on/off current ratio degrades noise margin, and V_{TH} variation due to random dopant fluctuations (RDF) reduces robustness of circuits. Functional robustness can be maintained by removing high fan-in gates, series transmission gates, and dynamic logic [13]. Also, the effect of RDF variation on critical path delay can be reduced with deeper logic depth between pipeline stages [12].

Power conversion efficiency from varying high battery voltage (e.g. 3.8~4.2V in Fig. 2) and the supply voltage should be considered. A switched-capacitor DC DC converter is typically chosen for mm-scale sensors [14], compared to a buck converter with a bulky off-chip inductor. However, the switched-capacitor converter with coarse output voltage step has suffered from degraded power conversion efficiency with varying battery voltage. For this issue, recently proposed reconfigurable DC DC converters with fine output voltage step [15] can be a solution.

In additional to the energy-efficient microprocessor, dense memory is desirable since it enables infrequent data transmission and complex data processing. Also, low standby power consumption is required for longer lifetime of the sensor with the limited battery capacity. Flash memory is a good candidate with zero leakage. However, large write power using charge pumps dominates the total system power budget (e.g. 15mA during programming, M25P32, Micron).

Instead, a 10T SRAM shown in Fig. 9 can be used to achieve low leakage (e.g. 1.85fW/bit at 0.35V) [16]. A 6T writing and retention portion uses I/O transistors with high V_{TH} for leakage reduction. Also, a 4T read buffer has standard transistors for fast read operation while it is power-gated in standby mode.

V. Conclusion

In this paper, a biomedical chip for a syringe-injectable pressure sensor is explored. The target sensing system is $1.6\times2.0\times3.2mm^3$ with 1mmHg pressure measurement accuracy, where the battery can be recharged by photovoltaic cells and sustained for more than a week without energy harvesting. To meet the extremely limited power budget due to the size constraint, ultra-low-power circuit techniques are discussed. The miniaturized sensing system can help reduce patient pain and recovery time, decrease foreign body rejection, and allow the device to be placed in limited spaces

References

[1] L. Yu, et al., "Chronically Implanted Pressure Sensors: Challenges and State of the Field," *Sensors*, vol. 14, no. 11, pp. 20620-20644, Oct. 2014.

[2] I. E. Araci, et al., "An implantable microfluidic device for self-monitoring of intraocular pressure," *Nature Medicine*, vol. 20, no. 9, pp. 1074-1078, Sep. 2014.

[3] I. Lee, "Power management circuits for miniature sensor systems," Ph.D. dissertation, Dept. Electrical Eng., Univ. Michigan, Ann Arbor, MI, USA, 2014.

[4] W. T. Abraham, et al., "Wireless pulmonary artery haemodynamic monitoring in chronic heart failure: a randomised controlled trial," *Lancet*, vol. 377, no. 9766, pp 658-666, Feb. 2011.

[5] P-J Chen, et al., "Microfabricated Implantable Parylene-Based Wireless Passive Intraocular Pressure Sensors," *J. Microelectromech. Syst.* vol. 17, no. 6, pp. 1342-1351, Dec. 2008.

[6] E. Y. Chow, et al., "A Miniature-Implantable RF-Wireless Active Glaucoma Intraocular Pressure Monitor," *IEEE Trans. Biomed. Circuits Syst*, vol. 4, no. 6, pp. 340-349, Dec. 2010.

[7] S. Oh, et al., "Dula-slope capacitance to digital converter integrated in an implantable pressure sensing systme," *IEEE ESSCIRC* Sep. 2014, pp. 295-298.

[8] H. S. Gill and M. R. Prausnitz, "Does Needle Size Matter?," *J. Diabetes Sci. Technol.*, vol. 1, no. 5, pp. 725-729, Sep. 2007.

[9] W. Jung, et al., "An Ultra-Low Power Fully Integrated Energy Harvester Based on Self-Oscillating Switched-Capacitor Voltage Doubler," *IEEE J. Solid-State Circuits*, vol. 49, no. 12, pp. 2800-2811, Dec. 2014.

[10] K. Tanaka, et al., "A 0.026mm^2 Capacitance-to-Digital Converter for Biotelemetry Applications Using a Charge Redistribution Technique," *IEEE ASSCC*, Nov. 2007, pp. 244-247.

[11] H. Ha, et al., "A 160nW 63.9fJ/conversion-step Capacitance-to-Digital Converter for Ultra-Low-Power Wireless Sensor Nodes," *IEEE ISSCC*, Feb. 2014, pp. 220-221.

[12] B. Zhai, et al., "Theoretical and practical limits of dynamic voltage scaling," *DAC*, June 2004, pp. 868-873.

[13] Y. Lee, et al., "Ultra-low power circuit techniques for a new class of sub-mm^3 sensor nodes," *IEEE ICCC*, Sep. 2010.

[14] S. Bang, et al., "A Fully Integrated Switched-Capacitor Based PMU with Adaptive Energy Harvesting Technique for Ultra-Low Power Sensing Applications," *IEEE ISCAS*, May 2013, pp. 709-712.

[15] S. Bang, et al., "A fully interated successive-approximation switched-capacitor DC-DC converter with 31mV output voltage resolution," *IEEE ISSCC*, Feb. 2013, pp. 370-371.

[16] D. Kim, et al., "A 1.85fW/bit Ultra Low Leakage 10T SRAM with Speed Compensation Scheme," *IEEE ISCAS*, May 2011, pp. 59-72.